Journal of Aerosol Science 155 (2021) 105757

Contents lists available at ScienceDirect

Journal of Aerosol Science

journal homepage: http://www.elsevier.com/locate/jaerosci

Computational analysis of a 3D mucociliary clearance model predicting nasal drug uptake

Sriram Chari [a], Karthik Sridhar [a], Ross Walenga [b], Clement Kleinstreuer [a,*]

[a] Department of Mechanical & Aerospace Engineering, NC State University, Raleigh, NC, 27695-7910, USA
[b] Division of Quantitative Methods and Modeling, Office of Research and Standards, Office of Generic Drugs, Center for Drug Evaluation and Research, US Food and Drug Administration, Silver Spring, MD, USA

ARTICLE INFO

Keywords:
Mucociliary clearance
Nasal drug dissolution and absorption
CFD analysis of inhaled drug-aerosol transport and uptake
Mucus layer dynamics
3D modeling

ABSTRACT

Accurate and realistic predictions of the fate of nasally inhaled drugs help to understand the complex fluid-particle dynamics in the nasal cavity. Key elements of such a comprehensive numerical analysis include: (i) inhaled drug-aerosol transport and deposition with air-particle-mucus interactions; and (ii) mucociliary clearance (MCC) dynamics, including drug transport, dissolution and absorption for different nasal inlet conditions.

The open-source computational fluid dynamics (CFD) toolbox, OpenFOAM, has been employed for the development of the computer simulation model. As part of the design, a novel 3D meshing technique allows for the smooth capture of both the relatively large flow domain as well as the micron-size mucus layer. This efficient meshing strategy drastically reduces the overall meshing time from hours to a matter of minutes. The effect of pharmacokinetic characteristics of drugs on dissolution, subsequent uptake and clearance were analyzed. A method to impose a boundary-driven flow velocity was introduced in order to mimic the beating of the cilia. Several drug specific parameters, such as solubility, partition coefficient and particle size, were considered. The effects of particle distribution on MCC and uptake were simulated as well. The CFD predictions show that drugs with a high partition coefficient are absorbed rapidly. Similarly, drugs with higher solubility show an appreciable increase in cumulative uptake in the epithelium. Particle size, however, plays a more nuanced role in drug uptake. Specifically, smaller particles with their relatively large surface areas, tend to dissolve quicker and are absorbed more rapidly when compared to larger particles. However, after the initial steeper increase in cumulative uptake of the smaller particles, the difference in the uptake values for the two cases is negligible. Furthermore, the initial deposition locations in the nasal cavity play an important role in overall drug uptake. Particles deposited closer to the ciliated portion of the nasal cavity (i.e. the posterior region) were more readily absorbed when compared to particles deposited closer to the unciliated nasal vestibule.

1. Introduction

Many drugs are administered orally or via invasive procedures. As an alternative to these approaches, the nasal route for drug-aerosol delivery is an attractive approach to combat pathological conditions such as allergic rhinitis or nasal polyposis, migraines

* Corresponding author.
E-mail address: ck@ncsu.edu (C. Kleinstreuer).

https://doi.org/10.1016/j.jaerosci.2021.105757
Received 23 August 2020; Received in revised form 16 December 2020; Accepted 13 January 2021
Available online 4 February 2021
0021-8502/Published by Elsevier Ltd.

and other central nervous system disorders (Chapman et al., 2013; Dhuria et al., 2010). For example, direct delivery of corticosteroids to the nasal airways is one of the key treatment methods for allergic rhinitis symptoms. As the nasal epithelium is highly vascularized, it provides an attractive route for drug delivery to the systemic regions as well (Djupesland, 2013). If rapid absorption of the delivered drugs can be ensured at the nasal epithelium, this methodology enables a fast onset of action avoiding formulation breakdown in the digestive system and first-pass metabolism as well as other side effects.

Clearly, the efficiency of nasal drug delivery is highly dependent on the nasal spray device, drug formulation, inhalation conditions, and nasal geometry. Nasal-spray drugs may be formulated as either a homogeneous solution, a heterogeneous suspension, or a solid-particle suspension. In homogeneous solutions, the active drug is already dissolved in a carrier liquid, so that the droplets (after deposition on the liquid - airway surface) are easily absorbed into the epithelial tissue. However, for a heterogeneous suspension, where solid drug particles are dispersed within a carrier liquid or appear as dry powder, the absorption of the drug at the nasal epithelium is dependent on the dissolution of the suspended drug in the nasal mucus (Costantino et al., 2007). Most commercial nasal sprays are currently formulated as suspensions (Shah et al., 2015). If the delivered suspension, or solid drugs, are either very large or insoluble in the mucus, the nasal mucosa may act as a permeation barrier to high-molecular-weight therapeutics. This may cause insufficient dissolution that, together with mucociliary clearance, can push the drug into the gastrointestinal tract; thus, reducing the overall effectiveness of the drug (Arora et al., 2002; Ugwoke et al., 2005). Understanding the interaction of nasal-airway mucus with deposited particles can help drug formulation scientists avoid problems of low drug absorption and utilize this information to enhance drug transport through the mucus. Computational modeling tools can be utilized to study inhaled drug transport plus deposition and subsequently the effects of nasal mucociliary clearance (MCC), including drug dissolution and absorption. Such validated numerical results provide valuable insight for best device design and drug characteristics.

Despite recent advancements, challenges concerning the effective nasal administration of drugs persist. For example, the deposition in the posterior region of the nasal cavity, where the vascularized epithelium is located, is poor (Laube, 2007; Suman et al., 1999). It has been shown that particles trapped in the highly viscous mucus layer are moved via MCC action from the nasal cavity to the nasopharynx from where it is eventually swallowed (Shah et al., 2015). Nasal drug availability is highly dependent on the pharmacokinetic characteristics of the drug molecules, while drug uptake in the nasal cavity is limited by the solubility of the inhaled drug (Costantino et al., 2007; Hussain, 1998). In vitro and computational studies have shown that most of the deposition of nasal spray particles occurred in the anterior third of the nasal cavity. That region is covered with non-ciliated, squamous epithelium and hence does not contribute to the uptake of the dissolved drug. In fact, drugs deposit largely in the anterior third of the nasal cavity because of the irregular contours of the nasal airways, preventing most aerosol particles from penetrating into the middle meatus or superior turbinates (Laube, 2007). The anatomical barrier also results in an uneven deposition of particles in the unciliated portion of the nasal vestibule. These particles are then expelled out through the nostril during sneezing thus reducing the efficacy of the inhaled drug. Although MCC can translocate particles from the anterior to the posterior part of the nasal cavity, it cannot be relied upon to effectively redistribute the deposited particles to the middle meatus from the unciliated nasal vestibule.

Several studies, both computational (Calmet et al., 2018; Inthavong et al., 2006; Kimbell et al., 2007; Kleinstreuer & Zhang, 2010; Shi et al., 2007) and experimental (Cheng et al., 1996, 2001; Kelly et al., 2004) have explored the deposition patterns of drug aerosols in the nasal cavity. However, these studies do not account for the dissolution and subsequent absorption of these deposited drug particles. There are some studies that have evaluated the absorption of vapor in the upper airways providing specific uptake rates (Kimbell & Subramaniam, 2001; Tian & Longest, 2010; Zhang et al., 2006); but they do not address the behavior of these soluble compounds after wall deposition.

Most computational MCC studies have assumed simplified geometrical structures. For example, Kirch et al. (2011 and 2012) considered interaction of deposited particles with the mucus and simulated the clearance of the particles in a 2-D domain. Rygg and Longest (2016) and Rygg et al. (2016a) and (2016b) focused numerically on dissolution, absorption and clearance of drug-aerosols in the nasal mucosa. Their steady-state deposition data was then exported into a planar mucus layer of 10-μm thickness. For computational ease, they considered the inner nasal walls to be a flat (2-D) surface subject to steady laminar flow. They studied the MCC and dissolution of three different drugs as well as the uptake of drugs at the epithelial surface over time based on deposited parcels. It was found that the aerosol concentration in the mucus layer reduced from 100% to 40% in 30 min and then gradually reduced to 10% over the next 5.5 h. The findings were applied in another study to determine the kinetic constants for the drugs to estimate the systemic exposure (Rygg et al., 2016b). Shang et al. (2019) extended the work of Rygg and Longest (2016) by retaining the topological features of the nasal cavity in the form of a 3D surface-shell model. They studied the development of flow features within the mucus layer but did not analyze the drug uptake predictions at the mucus-epithelium interface. In addition, only the gel layer with an average viscosity of 12 Pa-s was considered whereas the mucus layer is actually composed of a viscous gel layer and a *sol* layer containing the periciliary fluid (see Section 2.1 for more details). In principle, the gel layer is propelled forward due to metachronal waves generated by cilia. In order to accommodate this motion, Shang et al. (2019) and Rygg and Longest (2016) introduced a uniform mass source to ensure an average velocity of 6 mm/min. Presently we consider an actual 3D model of the mucus layer and move the gel layer forward by imposing a wall-driven velocity at the gel- and *sol*-layer interface. We also model the gel layer and *sol* layer separately which was not done in earlier computational works, thereby adding to realism with the present CFD model.

In summary, the objective of this study is to develop a comprehensive 3D MCC model using CFD to predict the dissolution, clearance, and absorption of drug suspensions in the nasal cavity. The flow field was validated based on in vitro data to establish confidence in the proposed MCC model. The accuracy of the MCC rate predictions was assessed through comparisons with an in vivo study (Shah et al., 2015) measuring the clearance of radiolabel tracers from the nasal cavity to the nasopharynx. In a nasal spray device, the excipient serves to transport undissolved drug particles in the nasal cavity. This 3D MCC model was employed to analyze the fate of these undissolved particles once they are lodged in the nasal cavity walls. The current study contributes to the development

of a CFD model for nasal drug delivery from the point of aerosol formation through epithelial absorption. Presently, an emphasis is placed on what happens to the suspended drug particles after deposition occurs, which is critical to understanding the dosimetry and targeting of nasal spray products.

2. Theory

The noninvasive nature of intranasal drug administration makes it a widely adopted technique for local and systemic delivery of therapeutic agents. The nasal mucosa, unlike other mucosae is easily accessible. Intranasal application circumvents the issues of gastrointestinal degradation and hepatic first pass metabolism of the drug (Bitter et al., 2011). The sticky mucus blanket presents the first line of defense and prevents foreign material from entering the deep lungs. However, drugs intended to hit a target site within the nasal cavity are also trapped in the highly viscous gel layer that reduces the efficacy of the drug. Soluble drugs, however, dissolve in the mucus layer, diffuse across the gel and *sol* layers and are eventually absorbed by the richly vascularized nasal epithelium. This enables the drug to enter the systemic regions through the blood stream without losing its efficacy.

2.1. Mucus layer

The nasal airway surfaces are lined with ciliated, columnar epithelial cells and covered with an airway surface layer (ASL) (Bustamante-Marin and Ostrowski, 2017). The ASL is composed of two distinct layers, i.e., an upper, highly viscous gel layer which is primarily composed of a tangled polymer network of mucin that traps inhaled foreign particles (Rubin, 2002). Then, a lower periciliary liquid (PCL) layer or *sol* layer is interposed between the mucus gel layer and the respiratory epithelium that lubricates the airway surfaces and facilitates ciliary beating for effective MCC (Knowles & Boucher, 2002). The *sol* layer is composed of water with electrolytes, serum proteins, immunoglobulins, and lipids. A thin layer of surfactant separates the gel and *sol* layers. Experimental studies have shown that at low shear rates, the viscosity of the fluid in the gel layer is as high as 10,000 times that of water (Tlaskalova--Hogenova et al., 2005) due to the overlapping adhesive mucin fibres present in the gel layer. Additionally, it has been observed that a gel viscosity when close to 12 Pa.S is optimal for MCC (Puchelle et al., 1987). The mucus layer is 5–20 μm thick (Gizurarson, 2015; Ugwoke et al., 2005) with the upper gel layer being 0.5–5 μm thick while the thickness of the lower *sol* layer ranges from 7 to 15 μm (Quraishi et al., 1998). The coordinated interaction between all these components of the ASL is paramount for effective MCC. Cilia are specialized structures present in the *sol* layer that provide the thrust necessary to transport inhaled particles lodged in the mucus layer

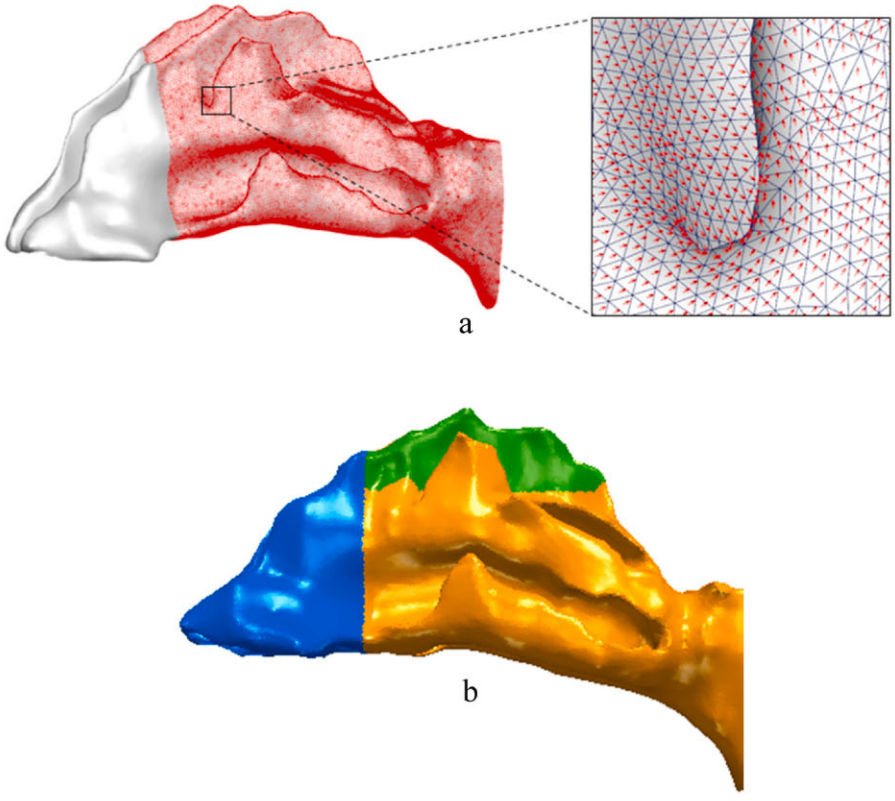

Fig. 1. a: Left: Tangential velocity of 6 mm/min imposed on the posterior region of the mucus layer. Right: Vectors (red) are imposed at the cell centers and follow the contours of the irregular 3D domain. 1b: The mucus layer geometry is divided into three distinct subdivisions: 1) nasal vestibule (blue); 2) ciliated posterior region (orange); 3) olfactory region (green). (For interpretation of the references to colour in this figure legend, the reader is referred to the Web version of this article.)

towards the nasopharynx. To accomplish this, the cilia beat in a whip-like manner producing metachronal waves at a beat frequency that has multiple physiological regulators (Bustamante-Marin and Ostrowski, 2017). The ASL height is assumed to remain constant because of the constant secretion of mucus from the goblet cells into the PCL layer and eventually into the upper gel layer (Shang et al., 2019).

2.2. Nasal geometry

The nasal cavity model used for this study was developed from MRI scans of the nose of a healthy, 53-year-old, non-smoking male (weighing 73 kg, 173 cm tall), provided by the Chemical Industry Institute of Toxicology (CIIT, Research Triangle Park, NC; also refer to Kelly et al. (2004a), Shi et al. (2008, 2007), and Shi (2007)). The image file was then processed and surface-smoothed to develop a computer-aided design (CAD)-like geometry file (Shi et al., 2007a). The nasal surface was then extruded by 10 μm to represent the gel layer. Another extrusion of 10 μm from the surface of the gel layer represented the *sol* layer. The model was divided into three different zones based on mucus producing characteristics of different regions inside the mucus layer. The anterior third of the nasal cavity called the nasal vestibule (NV) is unciliated and composed of keratinized squamous epithelial cells (Marttin et al., 1998). A free slip boundary condition was imposed at the air-gel and gel-water interfaces in this region. Experimental studies have shown that average mucus velocity in the posterior nose is around 6–7 mm/min (Davis & Illum, 2003; Ugwoke et al., 2005). To satisfy this condition, a tangential velocity of 6 mm/min was imposed on the surface of the mucus layer separating the gel and *sol* layers. As it is an irregular 3D computational domain, the applied tangential velocity follows the contours of the mucus layer in the direction of flow velocity as shown in Fig. 1a. The respiratory mucosa produces an average of 2 l mucus per day (Beule, 2010) of which around 15 ml is produced in the nasal cavity and transported to the nasopharynx (Arora et al., 2002). Also, since there is a large production of mucus in the maxillary sinus region near the olfactory (Halama et al., 1990), a normal velocity equal to 3×10^{-4}mm/min was introduced from each cell in the olfactory region lining the epithelial membrane. An outflow boundary condition is imposed at the nasopharynx and all remaining boundaries are assigned a free slip condition. In Fig. 1b, the *blue* region represents the unciliated nasal vestibule, the *orange* region represents the ciliated posterior region and the *green* region at the top is the olfactory region where the epithelium is lined with goblet cells responsible for mucus secretion.

2.3. Nasal cavity and mucus layer meshing

Considering the complexity and variability of the nasal geometry, it may not be prudent to generate a 3D mucus layer overlapping the airflow domain of the nasal geometry, partly because the process is very computer-resource intensive. Hence, we developed a tool in the open source CFD solver OpenFOAM v1706 (OpenCFD Ltd., Bracknell, United Kingdom) by modifying the *extrudeMesh* meshing utility to offset the surface mesh to the desired thickness without compromising the accuracy of the geometry. Utilizing the parallel computational capability of OpenFOAM, we were successful in offsetting the nasal geometry in a fraction of the time compared to the other meshing software platforms. With the OpenFOAM utility, a mesh comprising nearly 2 million elements was generated in about 2 min compared to over 30 min it takes to generate the same mesh on a Dell workstation powered by a 3.33 GHz Intel Xeon processor. The OpenFOAM utility tool operates on the patches along the boundary and extrudes the boundary front by a predefined distance along the outward pointing normal to the specific boundary. This provided an individual surface for the mucus layer, which could be exported as a surface and later meshed. Fig. 2 shows the nasal cavity with the offset mucus layer. Two separate regions are depicted where the region in dark gray is the original nasal surface and the region in light gray represents the new offset surface. The inset figure shows the two surfaces connected by a 20 μm thick surface (shown in magenta) which represents the mucus layer.

2.4. Drug dissolution and absorption modeling

A customized and improved Lagrangian particle tracking (LPT) solver called *dissolutionTransportFoam* was developed in OpenFOAM to track individual particles in the mucus layer and account for their size reduction owing to dissolution and later absorption.

The particles in the mucus layer are subjected to dissolution, which effectively means that the particle size will reduce with the passage of time. With this as the primary objective, it became necessary to modify the existing phase change model (evaporation model) in OpenFOAM to account for this phenomenon. The suspended drug particles dissolve according to the Noyes – Whitney mass

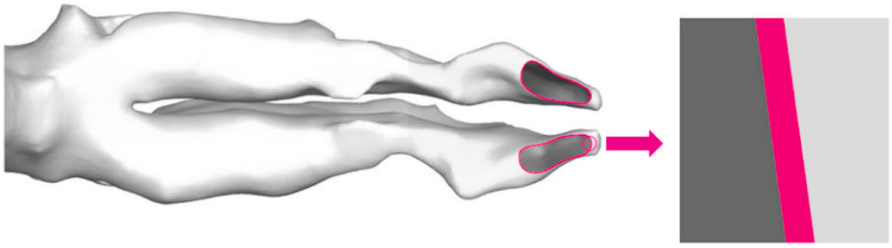

Fig. 2. Nasal geometry and mucus layer offset. Inset: Mucus layer (magenta) separates the nasal surface exposed to air (dark gray) and the epithelium (light gray).

transfer equation as they move through the nasal cavity, i.e.

$$\frac{dm}{dt} = \frac{AD_{mucus}(C_s - C_b)}{h} \tag{1}$$

here, m is the mass of the drug (kg), A is the surface area of the particle (m^2), D_{mucus} is the diffusion coefficient of the dissolved drug in the mucus layer (m^2/s), C_s is the solubility of the drug (mg/ml), C_b is the concentration of the dissolved drug in the bulk phase (mg/ml) and h is the diffusion layer thickness (m). The drug solubility, C_s is taken from the product information brochure for the respective drugs. The bulk phase concentration, C_b is updated by the solver during run time to mimic the constantly changing mucus layer environment. The diffusion layer thickness, h, which is approximated as the radius of the particle for particle radius <30 μm (Sugano et al., 2007) and the surface area, A change with time as the drug dissolves.

The LPT solver involves tracking the path of each particle in the domain until a certain condition is satisfied. The bulk fluid then advects the dissolved drug in the mucus layer by solving the scalar transport equation. The equations that are used are a combination of Newton's second law and a system of Navier - Stokes (N–S) equations. Specifically, drug-aerosol transport follows:

$$\frac{dx_{p,i}}{dt} = u_{p,i} \tag{2}$$

and

$$m\frac{du_p}{dt} = \sum F \tag{3}$$

For each particle, the above equation can be written as:

$$m\frac{du_{p,i}}{dt} = m_p\frac{(u_{f,i} - u_{p,i})}{t_p} + (\rho_p - \rho_f)g \tag{4}$$

$$t_p = \frac{4}{3}\frac{\rho_p {d_p}^2}{\rho_f C_D |u_{f,i} - u_{p,i}|} \tag{5}$$

t_p is the particle response time and is used to characterize the response time of the particle to sudden changes in the flow field.

Once the particle size reduction due to dissolution is computed, the dissolved drug is advected according to the convection – diffusion equation as given below.

$$\frac{\partial}{\partial t}(\rho Y_i) + \nabla \cdot (\rho \overrightarrow{v} Y_i) = \nabla \cdot (\rho D_{i,m} \nabla Y_i) + S_i \tag{6}$$

here, ρ is the density of the bulk fluid, Y_i is the mass fraction of species i, $D_{i,m}$ is the diffusion coefficient of the dissolved drug, S_i is the source term which accounts for the dissolution of the drug in the bulk fluid.

2.5. Uptake in the epithelial membrane

When the drug reaches the epithelial lining, uptake of the drug occurs. Since the absorption of the drug in the anterior third of the nose is minimal, a zero gradient boundary condition was applied in this region (Rygg & Longest, 2016). The posterior part of the nose is covered with the respiratory and olfactory epithelium where significant drug uptake occurs. Here, a mixed boundary condition was employed. The mass conservation at the interface separating the mucus layer and the epithelium is given by

$$D_{mucus}\frac{\partial C_{mucus}}{\partial x_n} = D_{epi}\frac{\partial C_{epi}}{\partial x_n} \tag{7}$$

here, D_{mucus} and D_{epi} are the drug diffusion coefficients in the mucus layer and the epithelium respectively. Since the epithelium represents a lipid phase and the mucus layer represents an aqueous phase, an octonol/water equilibrium partition coefficient was used (Rygg & Longest, 2016), given as:

$$K_{o/w} = \frac{C_{epi}}{C_{mucus}} \tag{8}$$

Assuming a linear concentration profile in the epithelium and zero concentration within the cell, a combination of the above two equations results in a mixed or Robin boundary condition in the epithelium:

$$\frac{\partial C_{mucus}}{\partial x_n} - \frac{D_{epi}K_{o/w}}{D_{mucus}t_{epi}}C_{mucus} = 0 \tag{9}$$

Here, t_{epi} is the thickness of the epithelial membrane.

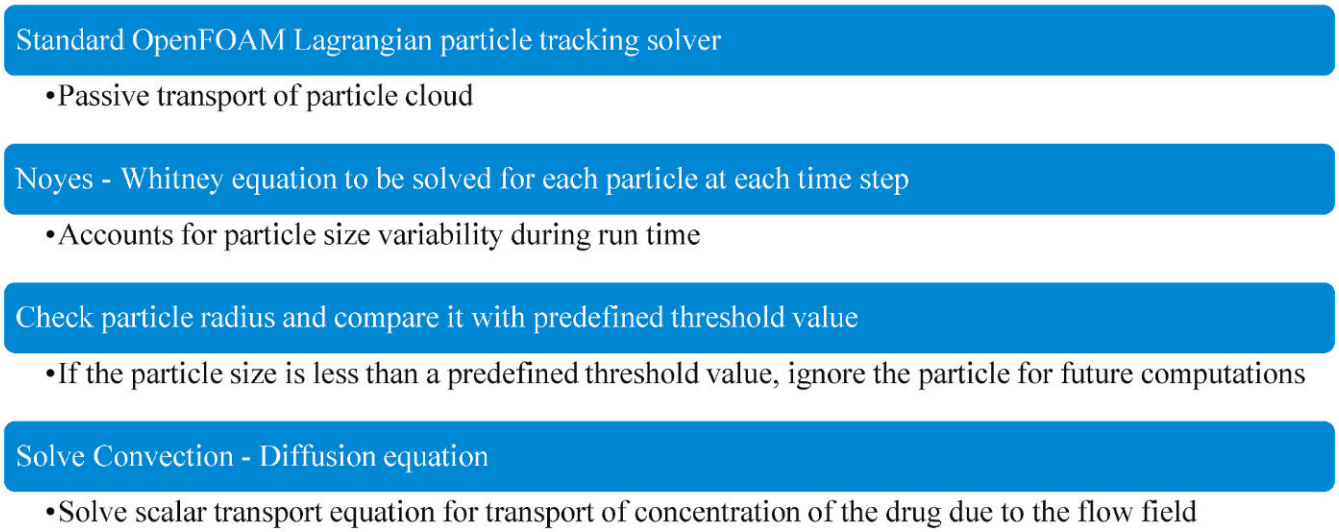

The flowchart highlights the different functionalities added to the base OpenFOAM LPT solver so that it can account for size variation of the particles due to dissolution and the subsequent transport of the dissolved drug with the bulk flow. To account for size variability of the drug particle during run time, the Noyes – Whitney equation (see Equation (1)) was added as a functional module which was coupled with the base LPT solver. The dissolved drug is finally advected by the bulk fluid, which is accounted for by solving the scalar transport equation (see Equation (6)).

We have considered three drugs in this computational study: Mometasone furoate (MF), Flunisolide (FN) and Ribavirin (RB). We have chosen these three drugs because MF is used in a nasal spray (Nasonex), FN is used in nasal sprays to treat sinusitis (Afrin) and RB is used as an antiviral drug (Virazole). Since the effective molecular radius of each of these compounds is very small, we assume that the diffusion coefficient of the drug in the mucus layer is approximately equal to its diffusion coefficient in water (Cu & Saltzman, 2009). Similarly, the solubility of the drug in water was used for the Noyes – Whitney mass transfer equation. The diffusion coefficient was computed using the Hayduk and Laudie equation (Hayduk & Laudie, 1974). Parameter values for the three drugs are given in Table 1.

The solubility value for MF was taken from Arora et al., 2010 and solubility for FN is taken from the Nasonex product monograph (Merck & Co,). All other values in Table 1 were obtained using the PubChem identification numbers (CID) of the drugs (National Center for Biotechnology Information, 2020; National Center for Biotechnology Information, 2020a; National Center for Biotechnology Information, 2020b).

3. Numerical method

The fluid-particle flow dynamics as well as the subsequent particle dissolution and absorption simulations were carried out using OpenFOAM, which is an open-source software written in C++. The mucus flow was simulated using the *simpleFoam* solver with the convergence criteria set at 10^{-4} for pressure and 10^{-5} for velocity. The converged flow field was then used to simulate the uptake of the drug in the epithelium. For simulating drug dissolution, a customized solver called *dissolutionTransportFoam* was developed based on the existing *scalarTransportFoam* module. It is capable of solving the advection-diffusion equation, track particles, and handle dissolution. A C++ code was written to incorporate the Robin boundary condition (see Equation (9)) at the boundary where uptake occurs. The Noyes-Whitney equation was coded in the customized solver to simulate the dissolution process. The residuals for the concentration field were required to drop to sufficiently low values (10^{-4}) at each time step. The uptake simulations were run for 5400 s with a time step of 0.1 s.

A grid independence study was done to determine the mesh resolution required to obtain computationally accurate results. Three different mesh configurations were analyzed: 5 mesh cells across the thickness of the mucus layer (≈0.95M elements), 10 mesh cells

Table 1
Pharmacokinetic properties of inhaled drugs.

	MF (CID 441336)	FN (CID 82153)	RB (CID 37542)
Molar mass (g/mol)	521.4	434.5	244.2
Molar volume (cm^3)	380	330	120
D_{mucus} (cm^2/s)	4.6×10^{-6}	4.9×10^{-6}	9.1×10^{-6}
Solubility (mg/ml)	0.02	0.2	20
Partition coefficient ($K_{o/w}$)	5000	2	0.005

across the mucus layer thickness (≈2M elements) and 15 cells across the mucus layer thickness (≈3M elements).

Fig. 3, shows that the 5-layer mesh does not compare well the in vivo results reported in Shah et al., 2015. The 10-layer mesh containing roughly 2M elements adequately captures the mass remaining in the nasal cavity as the data points obtained from simulations fall within the error bars reported in Shah et al., 2015. Refining the mesh by a factor of 1.5 results in only a negligible change in the mass remaining in the nasal cavity. To strike a balance between computational cost and solution accuracy, the mucus layer mesh used for the uptake simulations in this study consists of nearly 2 million tetrahedral elements (10 cells across the mucus layer thickness). This element size was sufficient to capture the flow field accurately and consequently provided stable uptake results.

3.1. Velocity validation

To validate the accuracy of the velocity field obtained from the proposed 3D mucus model, inert particle clearance data from the nose obtained from simulations was compared with in vivo data reported by Shah et al. (2015). In this in vivo study, radiolabel tracers were injected as nasal sprays which deposited on the walls of the nasal cavities. After 15 min, they found that 60% of the tracers were removed, consistent with other studies (Naclerio et al., 2003; Bacon et al., 2012) that reported a similar removal percentage. Since the radiolabel tracers administered were not absorbed, they concluded that this removal must be from MCC, confirming deposition to the ciliated posterior regions beyond the nasal valve. The initial positions of the tracers reported by Shah et al. (2015) were used to define the initial positions of inert particles for simulations conducted in this study. About 60% of the inert particles were injected from the posterior, ciliated region and 40% were introduced from the non-ciliated NV region. A transient simulation tracking the trajectory of these inert particles was then run for a duration of 6 h, consistent with the in vivo study. The mass remaining in the computational domain was calculated and compared with the value reported in the in vivo study.

Table 2 gives a comparison between the computational and experimental values of the mass of the inert particles remaining in the nasal cavity with time. The computational values compare well with those observed in the experimental study. Based on this evidence, it can be concluded that the velocity field obtained from the CFD model is expected to accurately represent MCC, including the effects of local changes in the velocity profile required to maintain a constant ASL thickness.

3.2. Dissolution & uptake validation

The dissolution model was validated by comparing the CFD simulation results with in vitro data presented by Franek et al. (2018). The experiment was conducted by first capturing 0.1–0.9% of the injected drug (2–4 mg) on a filter paper. These solid drug particles had a mass median diameter of 2.4 μm and an aqueous solubility of 0.024 mg/ml. These particles were then allowed to dissolve in a donor volume of 0.77 ml and permeate through the filter paper and Transwell membrane combination. The resulting profile of the mass of the drug leaving the donor and then permeating into the receptor was compared, i.e., as a percentage of the total mass, with the values reported in the Franek et al. (2018). It was found that the dissolution of drug particles takes over 2 h to complete, being in good agreement with the reported data (see Fig. 4a).

In a similar manner, the uptake boundary condition was validated by comparing the results of mass of drug permeating through the epithelium obtained from CFD simulations with in vitro data reported by Sadler et al. (2011). The in vitro drug absorption study was conducted by allowing 100 μl of a drug solution with partition coefficient 1.33 and concentration 0.0018 mg/ml, to permeate through an epithelial cell monolayer grown on a Transwell polyester membrane. The uptake validation was carried out using a mesh of the donor chamber with the uptake boundary condition imposed on the bottom surface i.e., the interface between the donor chamber and the epithelium. The aqueous diffusivity of the drug was calculated as $6 \times 10^{-10} m^2/s$ and applied throughout the domain, while an effective diffusivity of $2.1 \times 10^{-12} m^2/s$ was computed for the cell layer and Transwell membrane combination to account for its porosity. A low uptake rate of the drug solution was observed with less than 20% of the drug permeating in 40 min, which is

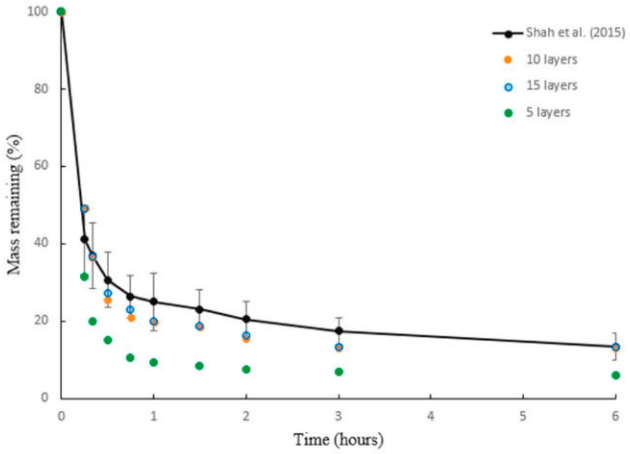

Fig. 3. Mass remaining in the nasal cavity as a percentage of the injected mass for different mesh configurations.

Table 2
Mean radiolabel remaining (standard deviation) in the nasal cavity as a percentage of the initial radiolabel tracers.

Time (min)	Mass remaining in the nasal cavity (%)	
	Shah et al. (2015)	Present study
0	100 (0)	100
15	41.11 (18)	49.27
20	37.02 (17)	36.45
30	30.71 (14)	25.50
45	26.42 (11)	21.15
60	25.00 (15)	19.76
90	23.04 (10)	18.61
120	20.54 (9)	15.56
180	17.37 (7)	13.15
360	13.32 (7)	13.14

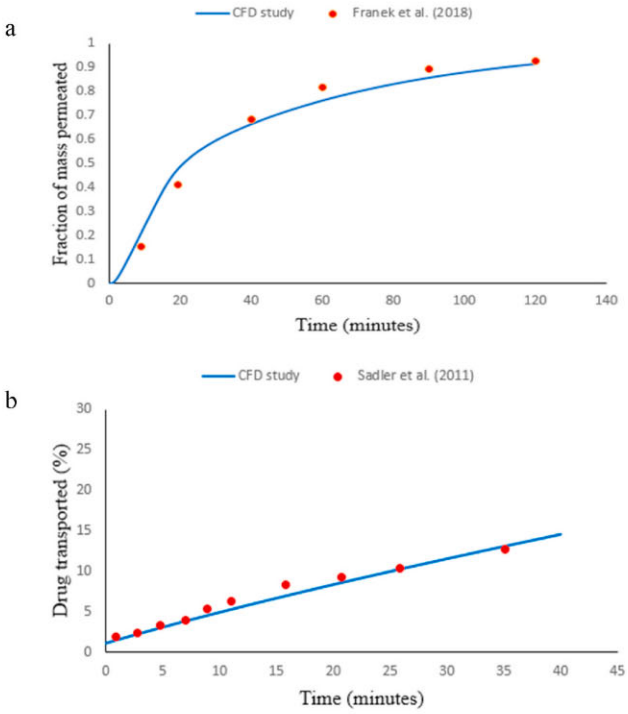

Fig. 4. a) Dissolution validation based on fractional drug mass permeated (Franek et al., 2018). b) Uptake validation based on drug transported across the cell layer as a percentage of the total dissolved drug mass (Sadler et al., 2011).

comparable to the in vitro study (see Fig. 4b).

As the values from both computer simulations are in good agreement with those provided in the in vitro studies, dissolution model and the uptake boundary condition are expected to predict drug dissolution and absorption in the nasal cavity with good accuracy.

4. Results and discussion

This study aims to realistically quantify the effect of drug formulation variables like solubility and partition coefficient on the dissolution and subsequent uptake in the nasal cavity for achieving a desired therapeutic effect. The goal is to enhance drug uptake through a combination of clearance, dissolution and absorption as well as drug targeting to maximize drug uptake. For visualization of the simulation results, the nasal cavity model was divided into three main regions: the anterior nasal vestibule (NV) which is unciliated, the middle passages (MPs), and the posterior nasopharynx. The MPs are further subdivided into different anatomical regions *viz* inferior meatus (IM), inferior turbinate (IT), middle meatus (MM), middle turbinate (MT) and the olfactory region (OLF).

The drug concentration and uptake in the subsequent sections were analyzed at a slice taken at approximately 60 mm from the nostril (see Fig. 5). This slice has a large cross section area which make it relatively easier to study trends in the concentration and uptake profiles across the thickness of the mucus layer. In addition, this slice is positioned in such a way that all seven sections of the MP detailed above are encapsulated. Its location closer to the nasopharynx helps in accounting for particles that might escape or get swallowed which otherwise would be difficult to estimate on a slice closer to the NV.

For nasally administered drugs through sprays, deposition in the NV region ranges from 70% to 85%, while the remaining drug particles deposit in the MP (Chen et al., 2020; Hallworth & Padfield, 1986; Shah et al., 2014). In Section 4.4, the effect of initial particle deposition location on subsequent uptake is discussed, but for all other cases (Sections 4.1–4.3) an 80/20 split is considered with 80% being deposited in the NV and the remaining 20% in the MP with the particles being randomly distributed on the two surfaces. The deposited particles are assumed to have an initial monodisperse diameter of 5 μm.

4.1. *Effect of partition coefficient*

The epithelium represents a lipid phase while the mucus layer represents an aqueous phase. The octonol-water partition coefficient ($K_{o/w}$) is an important parameter which characterizes the ability of the drug to move from the aqueous phase to the lipid phase. A high $K_{o/w}$ indicates an affinity for the lipid phase whereas a low $K_{o/w}$ represents a proclivity for the aqueous phase. In this section, three partition coefficients were considered, $K_{o/w} = 0.005$, 2, 5000. A $K_{o/w}$ of 5000 is representative of MF indicating a high relative affinity for the lipid phase (US FDA Nasonex product information guide) while a $K_{o/w}$ of 2 is representative of FN reflecting its water-soluble nature. A partition coefficient of 0.005 is indicative of a very hydrophilic drug such as RB. Being concerned with the effect of partition coefficient on drug uptake, the solubility of the drug in this case was kept fixed at 0.02 mg/ml. The effect of solubility on uptake is discussed later in Section 4.3.

Fig. 6 shows the uptake curves for different partition coefficients ($K_{o/w} = 0.005$, 2, 5000). The epithelial uptake profiles for $K_{o/w} = 2$ and 5000 are identical. This shows that although hydrophilic and lipophilic drugs are at opposite ends of the aqueous affinity spectrum, their cumulative uptake at the nasal epithelium is the same. The curves peak at around 3 min from the start of dissolution showing that initial uptake for both drugs is rapid. This can be attributed to the rapid initial dissolution of the sparsely distributed particles on the posterior surface of the nasal cavity that makes the drug readily available for uptake.

Fig. 7 shows the spatial and temporal evolution of the dissolved drug across the mucus layer. For $K_{o/w} = 0.005$, after 15 min, there is still dissolved drug available for uptake in the posterior part of the mucus layer. This is evidenced by the non – zero concentration values in the MP. With the passage of time, the dissolved drug is transported from the NV to the MP by the velocity induced in the NV due to MCC. The gradual decline in the concentration of the dissolved drug for $K_{o/w} = 0.005$ as shown in Fig. 7 suggests that the dissolved drug is slowly absorbed as it reaches the ciliated part of the nasal cavity which is lined with columnar epithelial cells.

For lipophilic drugs ($K_{o/w} = 2$ and 5000), there is an instantaneous uptake of the dissolved drug in the epithelium as soon as it reaches the MP. The near zero concentration values of the dissolved drug in the posterior part of the nasal cavity indicate this. Concurrently, velocity induced in the NV drives the dissolved drug into the MP. As soon as the drug reaches the MP, it is immediately absorbed by the epithelium.

It is observed that the predicted concentration at different sections in the ciliated part of the nasal cavity at $K_{o/w} = 2$ and 5000 is uniform throughout with a concentration close to zero. This also indicates that most of the drug is absorbed by the epithelium before it reaches the chosen slice. For $K_{o/w} = 0.005$, however, a noticeable variation in the concentration can be observed. This is depicted in Fig. 8 for different segments of the default slice. The drug concentration at the end of 1.5 h is very low in the IM and IT regions suggesting that drug uptake begins at the bottom of the nasal cavity. The MM and MT regions show higher drug concentration values which explains the lower uptake in these regions compared to the IM and IT regions. The OLF region has the highest drug concentration and conversely the lowest uptake implying that drugs designed to target the OLF region must have a relatively high partition coefficient if their solubility is low. The average velocity in the OLF region of the default slice is observed to be higher than in the remaining segments (see Fig. 8). This higher velocity, due to mucus injection from the goblet cells that line the OLF region, slows the uptake at the epithelium, because the dissolved drug is advected away. On the other hand, a lower velocity in the other segments allows the dissolved drug to be absorbed in the epithelium.

Chronic rhinosinusitis (CRS) is an inflammatory disorder of the paranasal sinuses. Olfactory dysfunction is a common manifestation of CRS and one of its primary diagnostic features (Gudis & Soler, 2016). The nasal drugs used to target inflammation in the sinuses like oxymetazoline (Afrin, Dristan; $K_{o/w} = 3.4$, Cs = 0.051 mg/ml), naphazoline (Privine; $K_{o/w} = 3.9$, Cs = 0.038 mg/ml), budesonide

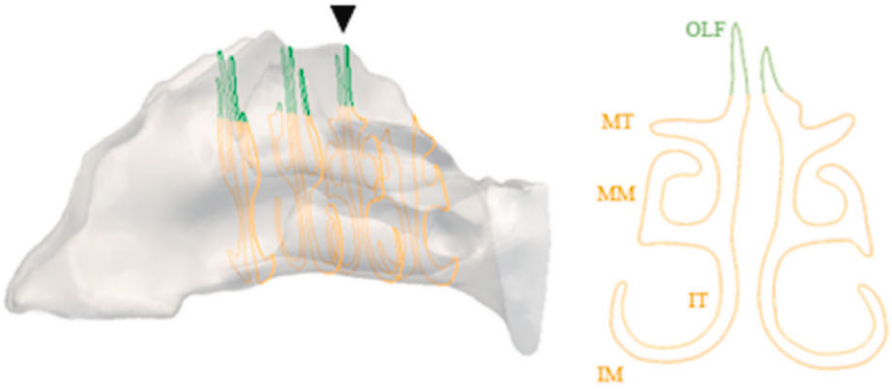

Fig. 5. Left: Mucus layer is divided into several slices. The default slice (60 mm from the nostrils) is indicated by the black marker. Right - Each slice is subdivided into a number of segments: IM, IT, MM, MT & OLF.

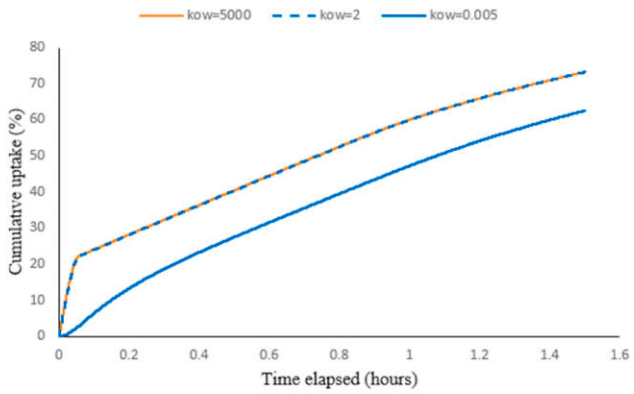

Fig. 6. Cumulative uptake as a percentage of the injected drug mass for different partition coefficients. (All cases ran with Cs = 0.02 mg/ml, d = 5 μm).

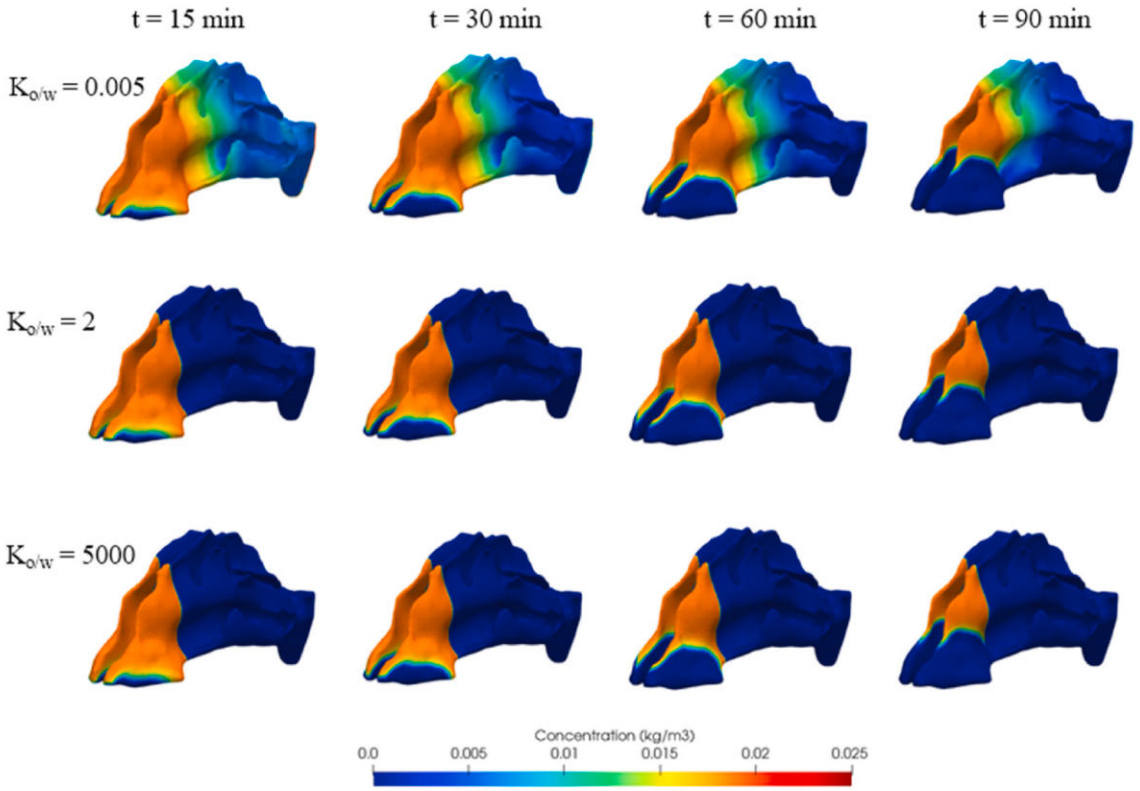

Fig. 7. Spatial and temporal evolution of concentration of the dissolved drug $K_{o/w}$ = 0.005, 2, 5000. (All cases are run with Cs = 0.02 mg/ml, d = 5 μm).

(Rhinocort Allergy; $K_{o/w}$ = 1.9, Cs = 0.047 mg/ml) and mometasone furoate (Nasonex; $K_{o/w}$ = 5000, Cs = 0.02 mg/ml) have partition coefficients higher than 1 which makes it easier for these drugs to get absorbed in the olfactory region of the nasal cavity. The partition coefficients and solubility for these drugs are taken from https://pubchem.ncbi.nlm.nih.gov. It can be observed from these segmental uptake patterns that for a given initial particle size, the drug continues to be absorbed in the posterior sections of the nasal cavity which means that the drug is absorbed over a greater surface area as the partition coefficient is decreased. Decreasing the partition coefficient of a drug increases the amount of drug reaching the posterior regions of the nasal cavity. Conversely, reducing the partition coefficient drastically can lead to reduced absorption and a large amount of drug being swallowed by the patient. This indicates the need to optimize the partition coefficient to suit the intended therapeutic purpose of the drug. This is valid for low solubility drugs and will be discussed in Section 4.3, i.e., how drugs with low partition coefficients but high solubility can also potentially be used to target the proximal regions of the nasal cavity.

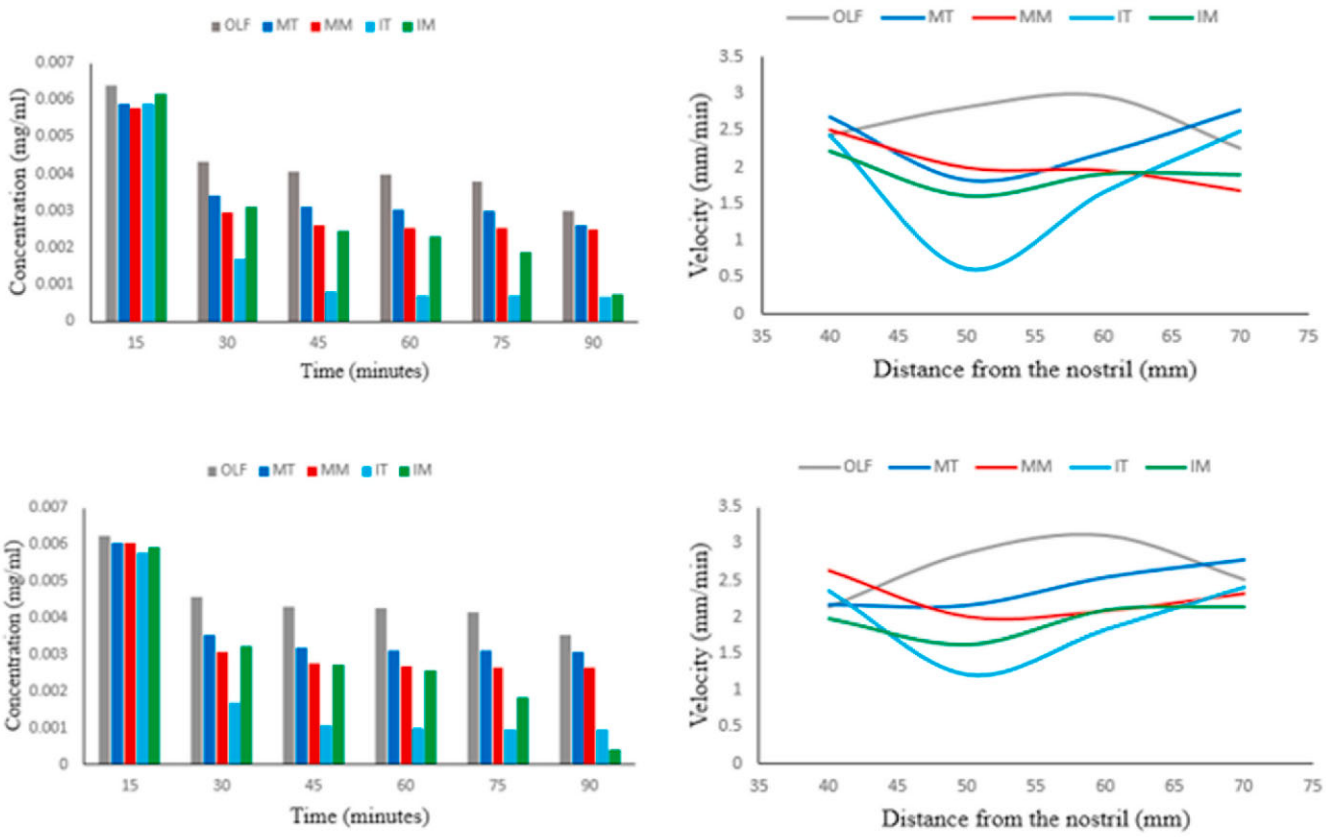

Fig. 8. Concentration values and velocity profiles in different nasal regions for Top: left nasal segment (LS) and Bottom: right nasal segment (RS).

4.2. *Effect of particle size*

According to the Noyes-Whitney equation (see Equation (1)), a decrease in particle size leads to an increase in the dissolution rate through an increase in the interfacial surface area and a decrease in the diffusion layer thickness surrounding each particle. The increase in initial uptake as seen in Fig. 9 can be attributed to this increase in the dissolution rate. The solubility of the drug is kept fixed at 0.02 mg/ml.

The smaller particles (3 μm) dissolve faster as explained above resulting in greater availability of the dissolved drug for uptake. The initial quick uptake corresponds to particles lodged in the posterior part of the nasal cavity lined with the ciliated epithelial cells which are absorbed as soon as they are available for uptake. This is more prominent in the case of 3 μm particles compared to the larger 5 μm particles (see Fig. 9). Once the initial surge in uptake subsides, there is not much difference in the cumulative uptake of the dissolved drug. Although the rate of dissolution for the two differently sized particles may be different, the amount of dissolved drug transported from the nasal vestibule to the posterior part of the nasal cavity is constant. This explains the similar uptake values for the 3 μm and 5 μm cases after the initial sharp rise.

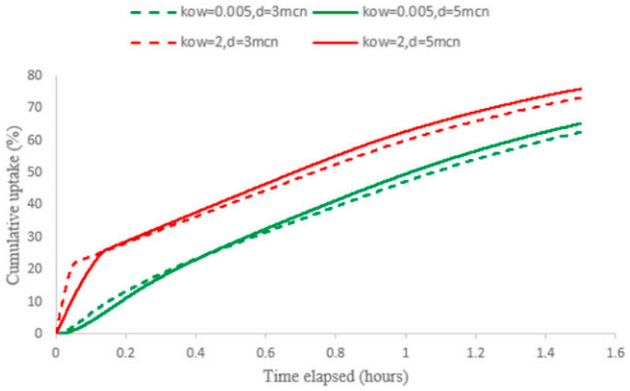

Fig. 9. Cumulative uptake as a percentage of the injected drug mass for different particle sizes and partition coefficients. (All cases are run with Cs = 0.02 mg/ml).

The initial, sharp increase in the cumulative uptake in the case of 3 μm particles over the larger 5 μm ones can be better understood by analyzing the temporal evolution of the dissolved drug available for uptake as shown in Fig. 10. This can be observed in all the highlighted segments of the nasal cavity (IM, MM, MT, OLF). With the passage of time, the drug concentration in these segments drops. This can be attributed to the absorption of the dissolved drug at the epithelium. Although the left and right segments are not symmetric, the drug concentration contours are comparable. The concentration contours are similar in all the nasal segments (IM, MM, MT, OLF) at any given time interval and hence, for the sake of brevity, only the contours in the MM are shown in Fig. 10 as a function of time till the time the uptake curve first peaks. The width of each segment in Fig. 10 represents the mucus layer with the right edge delineating the epithelium where drug-uptake occurs. Here, the solubility is 0.02 mg/ml and the partition coefficient is 2.

An increase in dissolution rate can also be explained by the reduction in the thickness of the diffusion layer around each particle (Bisrat & Nyström, 1988). The diffusion layer is essentially a hydrodynamic boundary layer surrounding the particle within which diffusion dominates. Hence, the Prandtl boundary layer equation can be used to explain the effect of this diffusion layer on the dissolution rate of the drug. The hydrodynamic boundary layer as described by Mosharraf and Nyström (1995) is as follows

$$h = k\sqrt{\frac{L}{V}} \tag{10}$$

where L is the characteristic length in the direction of flow, V is the velocity of the bulk fluid and k is a characteristic constant. As the particle size becomes smaller, the characteristic length L becomes smaller as well. This results in a thinner hydrodynamic layer surrounding the particle that inhibits diffusion, which is a rate limiting step. The net effect of a smaller particle size is an increase in the surface specific dissolution rate which is particularly pronounced for particles sizes less than 5 μm (Mosharraf & Nyström, 1995).

4.3. Effect of solubility

The effect of drug solubility on cumulative uptake of drugs is captured in Fig. 11. The results show that increasing the solubility by an order of magnitude has an appreciable impact on the epithelial uptake of the dissolved drug. This is due to the reduced availability of the drug with lower solubility (0.02 mg/ml) compared to the drug with higher solubility (0.2 mg/ml). It is also observed that due to lower solubility, around 25.5% of the 0.02 mg/ml drug remains undissolved after 1.5 h. In contrast, the higher solubility drug dissolves completely and hence, is completely available for uptake. In fact, since the drug with higher solubility is completely dissolved, it becomes difficult to target distal areas in the nasal cavity as there are no particles lodged in the mucus layer to carry them to the regions of interest closer to the nasopharynx. At higher solubility, the amount of drug exiting the back of the throat is negligible, as the particles have sufficient time to dissolve before reaching the nasopharynx. Following the trend seen in Fig. 11, one can expect an even higher rate of uptake for a solubility of 20 mg/ml. An initial particle size of 5 μm was chosen for these simulations.

Fig. 12 shows the spatial and temporal evolution of the dissolved drug across the mucus layer. For $K_{o/w} = 0.005$, after 15 min, there is still dissolved drug available for uptake in the posterior part of the mucus layer. This can be inferred from the non – zero concentration values in the MP. The gradual reduction in the concentration of the dissolved drug for $K_{o/w} = 0.005$ as shown in Fig. 12 suggests that the dissolved drug is slowly absorbed as it reaches the posterior part of the nasal cavity which is lined with columnar epithelial cells. For $K_{o/w} = 2$ and 5000, however, the dissolved drug is absorbed very quickly in the MP. Since the dissolution rate is very high compared to the case with Cs = 0.02 mg/ml, more drug is available for uptake within a short period of time. Subsequently, most of the drug gets absorbed within the first 30 min; however, for Cs = 0.02 mg/ml a noticeable amount of drug is still available for uptake even up to 90 min (see Fig. 7).

The cumulative uptake for each of the three drugs mentioned above viz. MF, FN and RB is shown in Fig. 13. The solubility and partition coefficients are taken from Table 1.

From Fig. 13, it can be seen that RB dissolves rapidly and is subsequently available for uptake. However, the rate of uptake for RB is lower than that for FN. This can be attributed to its very low partition coefficient. As discussed above, with drugs with high solubility, it

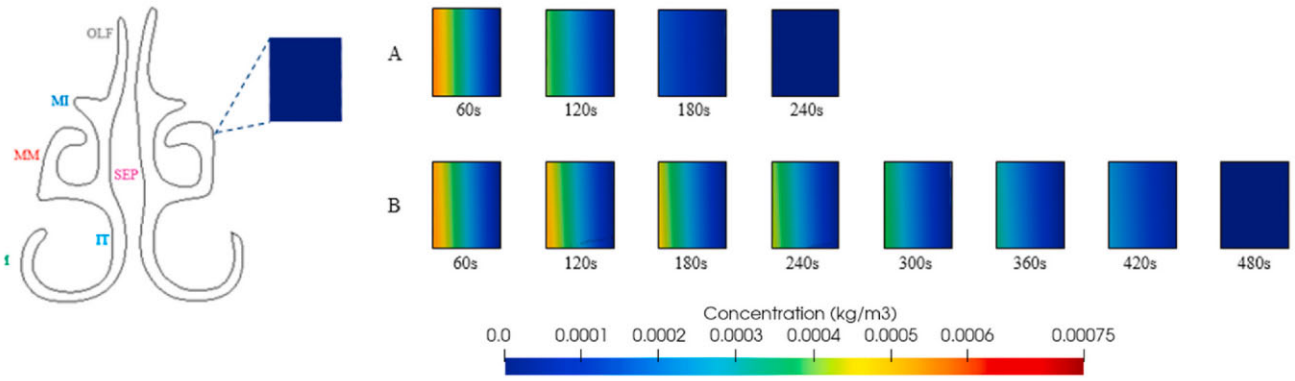

Fig. 10. Left: Different segments of the nasal cavity slice taken at 60 mm from the nostril. Right Top (A): drug concentration contours for 3 μm particles and bottom (B) for 5 μm particles.

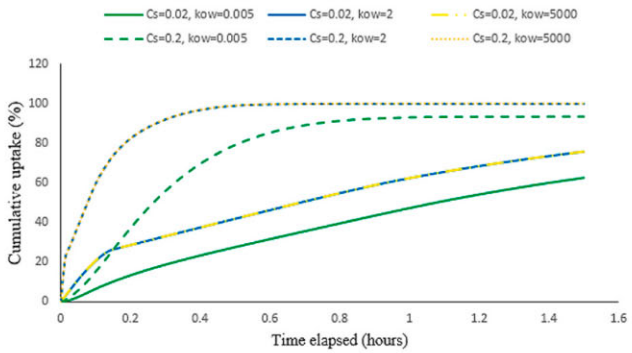

Fig. 11. Cumulative uptake as a percentage of the injected drug mass for different solubility and partition coefficients (All cases are run with d = 5 μm).

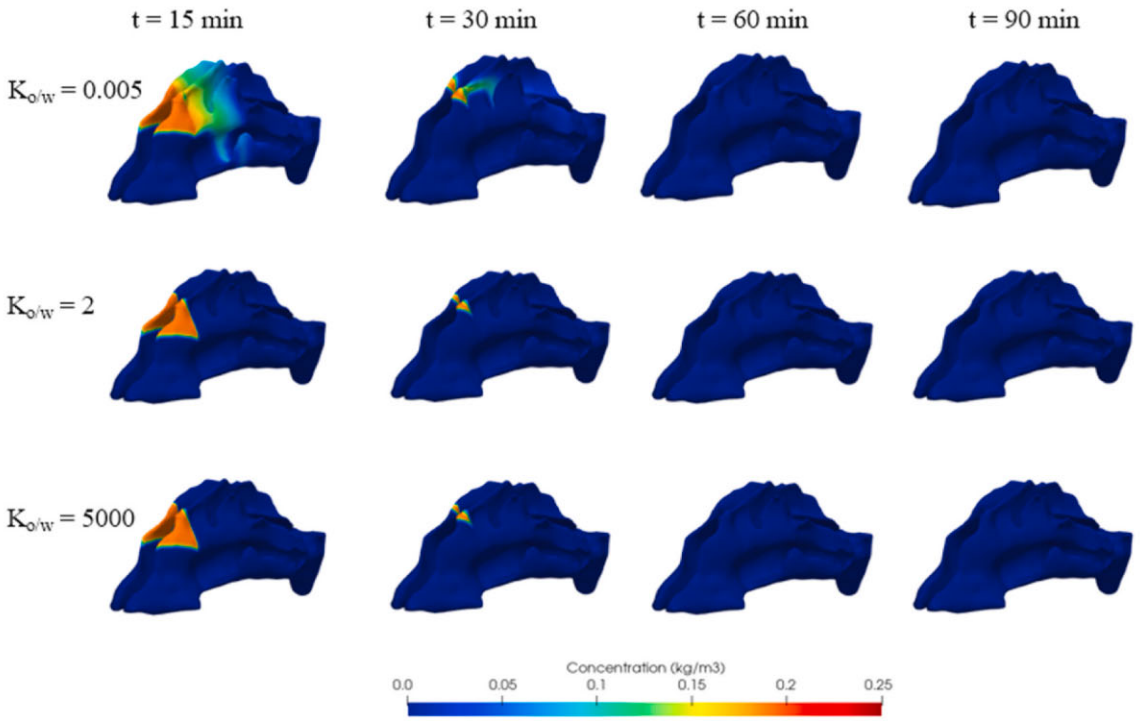

Fig. 12. Spatial and temporal evolution of concentration of the dissolved drug $K_{o/w}$ = 0.005, 2, 5000. (All cases are run with Cs = 0.2 mg/ml, d = 5 μm).

becomes difficult to target distal areas closer to the nasopharynx as there are very few particles lodged in the mucus layer to carry them to the regions of interest. Thus, even though RB has a very low partition coefficient, which is predicted to hinder uptake, the very high solubility of RB makes it viable for absorption in the proximal regions of the nasal cavity including the olfactory region. As such, RB is designed to target the olfactory bulb from where it reaches the brain (Colombo et al., 2011; Giuliani et al., 2018). The high solubility of RB enables its quick dissolution and results in a high concentration gradient across the epithelium, thus ensuring faster uptake before it can be expelled from the nasal cavity through the nasopharynx. MF is a potent corticosteroid with anti-inflammatory properties and is used in nasal sprays to treat rhinitis. The posterior areas of the nasal cavity are associated with rhinitis and polyposis inflammation (Shah et al., 2015). MF, with its low solubility, can be transported to these distal regions of the nasal cavity through MCC from where it is absorbed by the epithelium. Intranasal FN spray is used as an adjunct to oral antibiotic therapy to treat chronic rhinosinusitis (Meltzer et al., 1993). Rhinosinusitis is an inflammatory condition which afflicts the contiguous nasal and paranasal sinuses (Lund, 2008). Since FN is completely dissolved, no particle escapes through the nasopharynx and most of the drug is absorbed rapidly by the epithelium.

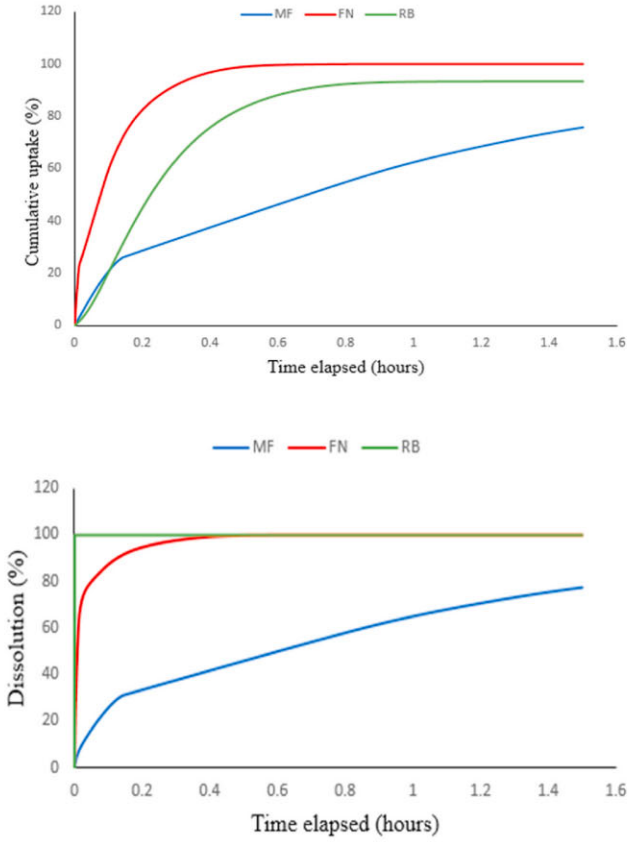

Fig. 13. Top: Cumulative uptake as a percentage of the injected drug mass for three different drugs: MF, FN, RB. Bottom: Dissolution as a percentage of mass injected for three different drugs: MF (Cs = 0.02 mg/ml, Ko/w = 5000), FN (Cs = 0.2 mg/ml, Ko/w = 2), RB (Cs = 20 mg/ml, Ko/w = 0.005). (All cases are run with d = 5 μm).

4.4. Effect of initial particle-deposition location

This section explores the impact of the initial deposition position of particles in the nasal cavity on drug uptake in the epithelium. The total drug mass deposited and available for dissolution and subsequent uptake is 45 μg. In this case, 3 μm particles are considered with three different particle distribution configurations: A: 80% in the NV & 20% in the posterior region; B: 50% in the NV & 50% in the posterior region and C: 20% in the NV & 80% in the posterior nasal cavity. The posterior region includes the ciliated epithelial region as well as the olfactory region. Here, the partition coefficient is 0.005 and the solubility is 0.02 mg/ml.

Fig. 14 compares the cumulative uptake trends for each of these three deposition patterns. The first case (highlighted in green) has a lower cumulative drug uptake than the other two cases. For the second case (highlighted in blue) where 50% of the drug is initially lodged in the posterior part, the initial quick rise in the cumulative uptake curve is higher than the case where only 20% is deposited in the posterior region. The third case (highlighted in pink) where 80% of the drug is initially trapped in the posterior part has the highest

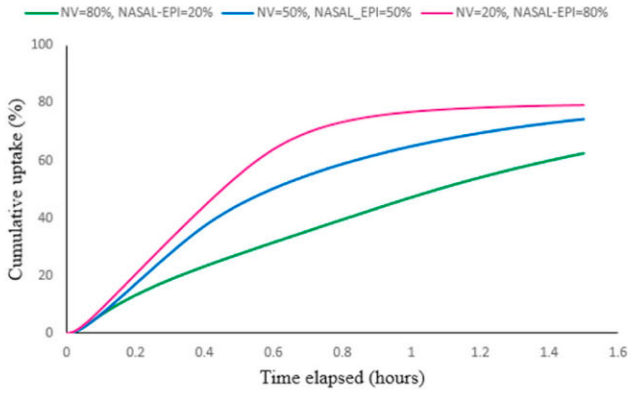

Fig. 14. Cumulative uptake as a percentage of the injected drug mass for different initial particle deposition concentrations. (All cases are run with $K_{o/w}$ = 0.005, Cs = 0.02 mg/ml, d = 5 μm).

uptake values at all measured time instances.

The spatial and temporal distribution of concentration for the three different particle distribution configurations discussed above is shown in Fig. 15. For case A, the total drug deposited in the posterior region is low compared to case B and case C. Once the drug deposited in this region dissolves and is absorbed, the remaining drug needs to be transported to the posterior region from the NV for drug uptake to continue. This is a slow process. Within the first 15 min, the dissolved drug from the posterior region is absorbed by the epithelium. For case B, since a greater proportion of the drug is initially lodged in the posterior part of the nasal cavity, a larger non – zero region can be seen. This implies that drug uptake continues at a faster rate before the slope of the cumulative uptake curve changes. It is only after 60 min that the dissolved drug from the MP is almost completely absorbed and the remaining uptake occurs due to transport of drug from the NV to the MP. This reasoning can be extended to case C as well. Here, 80% of the drug is initially deposited in the MP which suggests a faster rate of uptake than the other two cases.

5. Conclusions and future work

This numerical study quantifies the effect of drug solubility and partition coefficient on the dissolution and subsequent uptake of drugs in a realistic nasal cavity model. The goals were enhancement of drug uptake by analyzing a most suitable combination of clearance, dissolution and absorption processes, as well as drug targeting to maximize systemic drug uptake. The results provide insight into the possible effects of formulation variables like solubility, partition coefficient, and particle size on systemic exposure inside the nasal cavity.

The following conclusions can be drawn based on the computational results discussed in this paper:

- Partition coefficient: Increasing the partition coefficient from results in faster uptake of the dissolved drug in the epithelium. A lipophilic drug, having a high partition coefficient, is more effective when targeting proximal regions of the nasal cavity. In contrast, hydrophilic drugs, featuring low partition coefficients, are more prone to absorption in the posterior regions. Thus, based on the intended target site in the mucus layer, drugs with either high or low partition coefficients must be used.
- Particle size: Smaller particles dissolve quickly and are more readily available for uptake. Larger particles, on the other hand, have a larger diffusion layer surrounding them which inhibits dissolution. Consequently, the amount of drug available for epithelial uptake is limited.

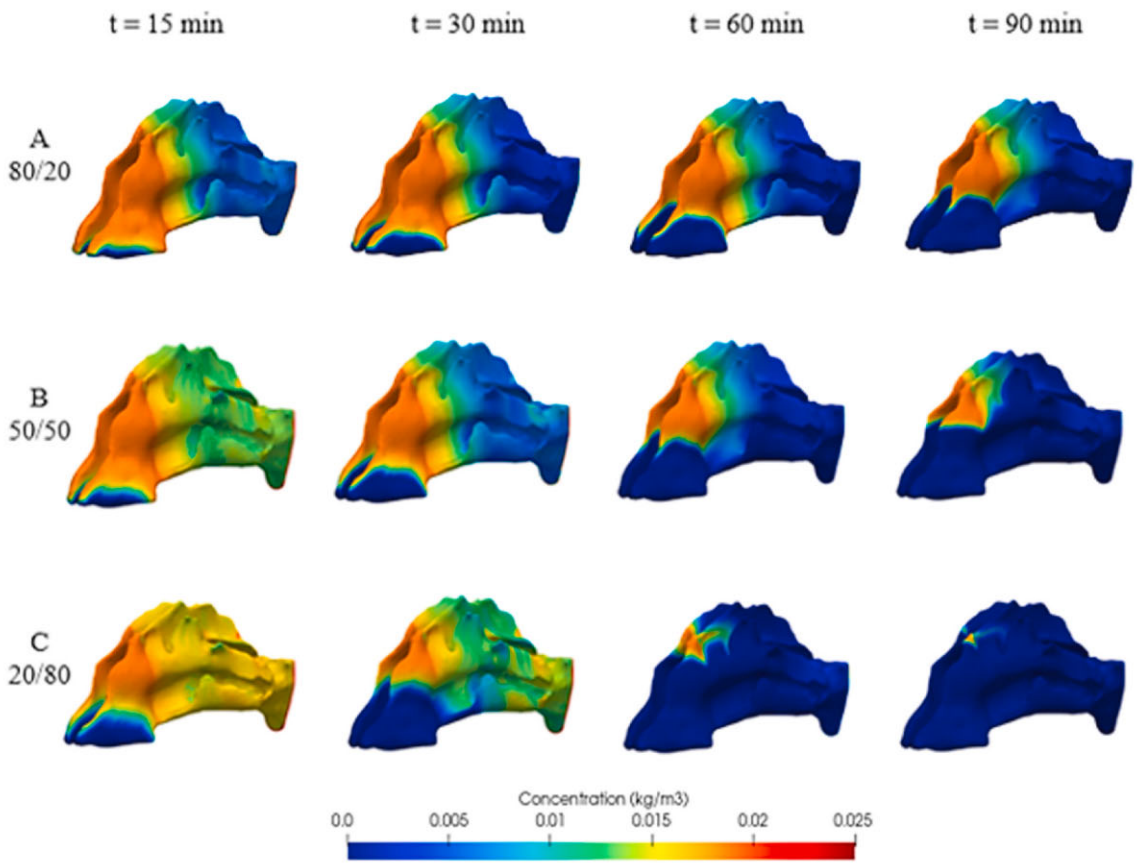

Fig. 15. Spatial and temporal distribution of drug concentration for different initial particle distribution configurations: A: 80/20; B: 50/50; C: 20/80 (All cases are run with $K_{o/w} = 0.005$, Cs = 0.02 mg/ml, d = 5 μm).

- Solubility: As solubility increases, the rate of dissolution increases as well as the subsequent absorption of the drug. Typically, drugs with higher solubility tend to dissolve completely. This ensures a higher uptake in the epithelium, but it also makes it difficult for the drug to reach the distal regions of the nasal cavity.
- Initial deposition location: The present results indicate that drug deposition in the unciliated anterior third of the nose precludes active translocation of those drugs to the posterior, distal regions *via* MCC. Drug absorption occurs only in the ciliated part of the nasal cavity.

Although the current CFD model lays a solid foundation for drug uptake predictions through the intranasal route, it has certain limitations. The airway surface layer (ASL) in this study consists of a gel layer and a *sol* layer. The gel layer is modeled as a Newtonian fluid with a high viscosity compared to the *sol* layer whose viscosity is 10,000 times lower than that in the gel layer. It has, however, been established that the mucus layer exhibits rheological complexities that cannot be captured by the Newtonian approximation, especially at high strain rates (Sedaghat et al., 2016). A number of analytical studies have been performed to determine the effect of mucus viscoelasticity on the mucociliary transport (Blake, 1972; Fulford & Blake, 1986; King et al., 1993; Sleigh et al., 1988; Smith et al., 2008). Viscoelastic models are convenient because they are easy to model and can capture the linear response of the mucus to small deformations (<2–3%) (Funk et al., 2000). They also can capture non–linear deformations experienced at higher strain rates.

This study assumed monodisperse particles for each simulation. However, commercial suspension formulations contain polydisperse suspended particles (Finlay & Darquenne, 2020). Finally, the model in its current form calculates the cumulative mass of the dissolved drug that is absorbed at the epithelium but does not calculate the plasma concentration profiles. This makes it difficult to fully assess the impact of formulation variable differences on in vivo performance of the drug. To address this limitation, a physiologically-based pharmacokinetics model is planned to simulate the amount of drug that enters both the epithelial cells and the systemic circulation. It will allow for a one-to-one comparison of nasal deposition profiles and blood concentration of the inhaled drugs.

Declaration of competing interest

The authors declare that they have no known competing financial interests or personal relationships that could have appeared to influence the work reported in this paper.

Acknowledgement

Funding was provided by Grant 1U01FD006537, from the Department of Health and Human Services, U.S. Food and Drug Administration. Views expressed in this manuscript do not necessarily reflect the official policies of the U.S. Food and Drug Administration, nor does any mention of trade names, commercial practices, or organization imply endorsement by the United States Government.

References

Arora, D., Shah, K. A., Halquist, M. S., & Sakagami, M. (2010). In vitro aqueous fluid-capacity-limited dissolution testing of respirable aerosol drug particles generated from inhaler products. *Pharmaceutical Research, 27*(5), 786–795.

Arora, P., Sharma, S., & Garg, S. (2002). Permeability issues in nasal drug delivery. *Drug Discovery Today, 7*(18), 967–975.

Bacon, R., Newman, S., Rankin, L., Pitcairn, G., & Whiting, R. (2012). Pulmonary and nasal deposition of ketorolac tromethamine solution (SPRIX) following intranasal administration. *International Journal of Pharmaceutics, 431*(1–2), 39–44.

Beule, A. G. (2010). Physiology and pathophysiology of respiratory mucosa of the nose and the paranasal sinuses. In *GMS current topics in otorhinolaryngology, head and neck surgery* (Vol. 9).

Bisrat, M., & Nyström, C. (1988). Physicochemical aspects of drug release. VIII. The relation between particle size and surface specific dissolution rate in agitated suspensions. *International Journal of Pharmaceutics, 47*(1–3), 223–231.

Bitter, C., Suter-Zimmermann, K., & Surber, C. (2011). *Nasal drug delivery in humans* (pp. 20–35). Topical Applications: Karger Publishers. and the Mucosa.

Blake, J. (1972). A model for the micro-structure in ciliated organisms. *Journal of Fluid Mechanics, 55*(1), 1–23.

Bustamante-Marin, X. M., & Ostrowski, L. E. (2017a). Cilia and mucociliary clearance. *Cold Spring Harbor Perspectives in Biology, 9*(4). a028241.

Calmet, H., Kleinstreuer, C., Houzeaux, G., Kolanjiyil, A. V., Lehmkuhl, O., Olivares, E., et al. (2018). Subject-variability effects on micron particle deposition in human nasal cavities. *Journal of Aerosol Science, 115*, 12–28.

Chapman, C. D., Frey, W. H., Craft, S., Danielyan, L., Hallschmid, M., Schith, H. B., et al. (2013). Intranasal treatment of central nervous system dysfunction in humans. *Pharmaceutical Research, 30*(10), 2475–2484.

Cheng, K., Cheng, Y., Yeh, H., Guilmette, R. A., Simpson, S. Q., Yang, Y., et al. (1996a). In vivo measurements of nasal airway dimensions and ultrafine aerosol deposition in the human nasal and oral airways. *Journal of Aerosol Science, 27*(5), 785–801.

Cheng, Y. S., Holmes, T. D., Gao, J., Guilmette, R. A., Li, S., Surakitbanharn, Y., et al. (2001). Characterization of nasal spray pumps and deposition pattern in a replica of the human nasal airway. *Journal of Aerosol Medicine, 14*(2), 267–280.

Chen, J. Z., Kiaee, M., Martin, A., & Finlay, W. H. (2020). In vitro assessment of an idealized nose for nasal spray testing: Comparison with regional deposition in realistic nasal replicas. *International Journal of Pharmaceutics*, 119341.

Colombo, G., Lorenzini, L., Zironi, E., Galligioni, V., Sonvico, F., Balducci, A. G., et al. (2011). Brain distribution of ribavirin after intranasal administration. *Antiviral Research, 92*(3), 408–414.

Costantino, H. R., Illum, L., Brandt, G., Johnson, P. H., & Quay, S. C. (2007). Intranasal delivery: Physicochemical and therapeutic aspects. *International Journal of Pharmaceutics, 337*(1–2), 1–24.

Cu, Y., & Saltzman, W. M. (2009). Mathematical modeling of molecular diffusion through mucus. *Advanced Drug Delivery Reviews, 61*(2), 101–114.

Davis, S. S., & Illum, L. (2003). Absorption enhancers for nasal drug delivery. *Clinical Pharmacokinetics, 42*(13), 1107–1128.

Dhuria, S. V., Hanson, L. R., & Frey, W. H. (2010). Intranasal delivery to the central nervous system: Mechanisms and experimental considerations. *Journal of Pharmaceutical Science, 99*(4), 1654–1673.

Djupesland, P. G. (2013). Nasal drug delivery devices: Characteristics and performance in a clinical perspective—a review. *Drug Delivery and Translational Research, 3*(1), 42–62.
Finlay, W. H., & Darquenne, C. (2020). Particle size distributions. *Journal of Aerosol Medicine and Pulmonary Drug Delivery, 33*(4), 178–180.
Fulford, G. R., & Blake, J. R. (1986). Muco-ciliary transport in the lung. *Journal of Theoretical Biology, 121*(4), 381–402.
Funk, J. R., Hall, G. W., Crandall, J. R., & Pilkey, W. D. (2000). Linear and quasi-linear viscoelastic characterization of ankle ligaments. *Journal of Biomechanical Engineering, 122*(1), 15–22.
Giuliani, A., Balducci, A. G., Zironi, E., Colombo, G., Bortolotti, F., Lorenzini, L., et al. (2018). In vivo nose-to-brain delivery of the hydrophilic antiviral ribavirin by microparticle agglomerates. *Drug Delivery, 25*(1), 376–387.
Gizurarson, S. (2015). The effect of cilia and the mucociliary clearance on successful drug delivery. *Biological and Pharmaceutical Bulletin, 14*.
Gudis, D. A., & Soler, Z. M. (2016). Chronic rhinosinusitis-related smell loss: Medical and surgical treatment efficacy. *Current Otorhinolaryngology Reports, 4*(2), 142–147.
Halama, A. R., Decreton, S., Bijloos, J. M., & Clement, P. A. (1990). Density of epithelial cells in the normal human nose and the paranasal sinus mucosa. A scanning electron microscopic study. *Rhinology, 28*(1), 25–32.
Hallworth, G. W., & Padfield, J. M. (1986). A comparison of the regional depesition in a model nose of a drug discharged from metered serosel and metered-pump nasal delivery systems. *The Journal of Allergy and Clinical Immunology, 77*(2), 348–353.
Hayduk, W., & Laudie, H. (1974). Prediction of diffusion coefficients for nonelectrolytes in dilute aqueous solutions. *AIChE Journal, 20*(3), 611–615.
Hussain, A. A. (1998). Intranasal drug delivery. *Advanced Drug Delivery Reviews, 29*(1–2), 39–49.
Inthavong, K., Tian, Z. F., Li, H. F., Tu, J. Y., Yang, W., Xue, C. L., et al. (2006). A numerical study of spray particle deposition in a human nasal cavity. *Aerosol Science and Technology, 40*(11), 1034–1045.
Kelly, J. T., Asgharian, B., Kimbell, J. S., & Wong, B. A. (2004a). Particle deposition in human nasal airway replicas manufactured by different methods. Part II: Ultrafine particles. *Aerosol Science & Technology, 38*(11), 1072–1079.
Kelly, J. T., Asgharian, B., Kimbell, J. S., & Wong, B. A. (2004b). Particle deposition in human nasal airway replicas manufactured by different methods. Part I: Inertial regime particles. *Aerosol Science and Technology, 38*(11), 1063–1071.
Kimbell, J. S., Segal, R. A., Asgharian, B., Wong, B. A., Schroeter, J. D., Southall, J. P., et al. (2007). Characterization of deposition from nasal spray devices using a computational fluid dynamics model of the human nasal passages. *Journal of Aerosol Medicine, 20*(1), 59–74.
Kimbell, J. S., & Subramaniam, R. P. (2001). Use of computational fluid dynamics models for dosimetry of inhaled gases in the nasal passages. *Inhalation Toxicology, 13*(5), 325–334.
King, M., Agarwal, M., & Shukla, J. B. (1993). A planar model for mucociliary transport: Effect of mucus viscoelasticity. *Biorheology, 30*(1), 49–61.
Kirch, J., Guenther, M., Doshi, N., Schaefer, U. F., Schneider, M., Mitragotri, S., et al. (2012). Mucociliary clearance of micro-and nanoparticles is independent of size, shape and charge—an ex vivo and in silico approach. *Journal of Controlled Release, 159*(1), 128–134.
Kirch, J., Guenther, M., Schaefer, U. F., Schneider, M., & Lehr, C. (2011). Computational fluid dynamics of nanoparticle disposition in the airways: Mucus interactions and mucociliary clearance. *Computing and Visualization in Science, 14*(7), 301–308.
Kleinstreuer, C., & Zhang, Z. (2010). Airflow and particle transport in the human respiratory system. *Annual Review of Fluid Mechanics, 42*, 301–334.
Knowles, M. R., & Boucher, R. C. (2002). Mucus clearance as a primary innate defense mechanism for mammalian airways. *Journal of Clinical Investigation, 109*(5), 571–577.
Laube, B. L. (2007). Devices for aerosol delivery to treat sinusitis. *Journal of Aerosol Medicine, 20*(s1), S5–S18.
Lund, V. J. (2008). Therapeutic targets in rhinosinusitis: Infection or inflammation? *The Medscape Journal of Medicine, 10*(4), 105.
Marttin, E., Schipper, N. G., Verhoef, J. C., & Merkus, F. W. (1998). Nasal mucociliary clearance as a factor in nasal drug delivery. *Advanced Drug Delivery Reviews, 29*(1–2), 13–38.
Meltzer, E. O., Orgel, H. A., Backhaus, J. W., Busse, W. W., Druce, H. M., Metzger, W. J., et al. (1993). Intranal flunisolide spray as an adjunct to oral antibiotic therapy for sinusitis. *The Journal of Allergy and Clinical Immunology, 92*(6), 812–823.
Merck & Co. Nasonex Product Monograph. https://www.merck.ca/static/pdf/NASONEX-PM_E.pdf.
Mosharraf, M., & Nyström, C. (1995). The effect of particle size and shape on the surface specific dissolution rate of microsized practically insoluble drugs. *International Journal of Pharmaceutics, 122*(1–2), 35–47.
Naclerio, R. M., Baroody, F. M., Bidani, N., Marcy De, T., & Penney, B. C. (2003). A comparison of nasal clearance after treatment of perennial allergic rhinitis with budesonide and mometasone. *Otolaryngology - Head and Neck Surgery, 128*(2), 220–227.
National Center for Biotechnology Information. (2020). PubChem compound summary for CID 82153, flunisolide. https://pubchem.ncbi.nlm.nih.gov/compound/Flunisolide.
National Center for Biotechnology Information. (2020a). PubChem compound summary for CID 441336, mometasone furoate. https://pubchem.ncbi.nlm.nih.gov/compound/Mometasone-furoate.
National Center for Biotechnology Information. (2020b). PubChem compound summary for CID 37542, ribavirin. https://pubchem.ncbi.nlm.nih.gov/compound/Ribavirin.
Puchelle, E., Zahm, J. M., & Quemada, D. (1987). Rheological properties controlling mucociliary frequency and respiratory mucus transport. *Biorheology, 24*(6), 557–563.
Quraishi, M. S., Jones, N. S., & Mason, J. (1998). The rheology of nasal mucus: A review. *Clinical Otolaryngology and Allied Sciences, 23*(5), 403–413.
Rubin, B. K. (2002). Physiology of airway mucus clearance. *Respiratory Care, 47*(7), 761.
Rygg, A., Hindle, M., & Longest, P. W. (2016a). Absorption and clearance of pharmaceutical aerosols in the human nose: Effects of nasal spray suspension particle size and properties. *Pharmaceutical Research, 33*(4), 909–921.
Rygg, A., Hindle, M., & Longest, P. W. (2016b). Linking suspension nasal spray drug deposition patterns to pharmacokinetic profiles: A proof-of-concept study using computational fluid dynamics. *Journal of Pharmaceutical Science, 105*(6), 1995–2004.
Rygg, A., & Longest, P. W. (2016). Absorption and clearance of pharmaceutical aerosols in the human nose: Development of a CFD model. *Journal of Aerosol Medicine and Pulmonary Drug Delivery, 29*(5), 416–431.
Sadler, R. C., Prime, D., Burnell, P. K., Martin, G. P., & Forbes, B. (2011). Integrated in vitro experimental modelling of inhaled drug delivery: Deposition, dissolution and absorption. *Journal of Drug Delivery Science and Technology, 21*(4), 331–338.
Sedaghat, M. H., Shahmardan, M. M., Norouzi, M., Nazari, M., & Jayathilake, P. G. (2016). On the effect of mucus rheology on the muco-ciliary transport. *Mathematical Biosciences, 272*, 44–53.
Regional deposition of mometasone furoate nasal spray suspension in humansShah, S. A., Berger, R. L., McDermott, J., Gupta, P., Monteith, D., Connor, A., & Lin, W. (Eds.). *Allergy and Asthma Proceedings, 36*(1), (2015), 48–57.
Shah, S. A., Dickens, C. J., Ward, D. J., Banaszek, A. A., George, C., & Horodnik, W. (2014). Design of experiments to optimize an in vitro cast to predict human nasal drug deposition. *Journal of Aerosol Medicine and Pulmonary Drug Delivery, 27*(1), 21–29.
Shang, Y., Inthavong, K., & Tu, J. (2019). Development of a computational fluid dynamics model for mucociliary clearance in the nasal cavity. *Journal of Biomechanics, 85*, 74–83.
Shi, H. (2007). *Numerical simulation of airflow, particle deposition and drug delivery in a representative human nasal airway model.* Raleigh, NC, USA: Ph.D. Dissertation, NC State University.
Shi, H., Kleinstreuer, C., & Zhang, Z. (2007). Modeling of inertial particle transport and deposition in human nasal cavities with wall roughness. *Journal of Aerosol Science, 38*(4), 398–419.
Shi, H., Kleinstreuer, C., & Zhang, Z. (2008). Dilute suspension flow with nanoparticle deposition in a representative nasal airway model. *Physics of Fluids, 20*(1), 013301.
Sleigh, M. A., Blake, J. R., & Liron, N. (1988). The propulsion of mucus by cilia. *American Review of Respiratory Disease, 137*(3), 726–741.

Smith, D. J., Gaffney, E. A., & Blake, J. R. (2008). Modelling mucociliary clearance. *Respiratory Physiology & Neurobiology, 163*(1–3), 178–188.
Sugano, K., Okazaki, A., Sugimoto, S., Tavornvipas, S., Omura, A., & Mano, T. (2007). Solubility and dissolution profile assessment in drug discovery. *Drug Metabolism and Pharmacokinetics, 22*(4), 225–254.
Suman, J. D., Laube, B. L., & Dalby, R. (1999). Comparison of nasal deposition and clearance of aerosol generated by a nebulizer and an aqueous spray pump. *Pharmaceutical Research, 16*(10), 1648.
Tian, G., & Longest, P. (2010). Development of a CFD boundary condition to model transient vapor absorption in the respiratory airways. *Journal of Biomechanical Engineering, 132*(5).
Tlaskalova-Hogenova, H., Tuckova, L., Mestecky, J., Kolinska, J., Rossmann, P., Stepankova, R., Kozakova, H., Hudcovic, T., Hrncir, T., & Frolova, L. (2005). Interaction of mucosal microbiota with the innate immune system. *Scandinavian Journal of Immunology, 62*, 106–113.
Ugwoke, M. I., Agu, R. U., Verbeke, N., & Kinget, R. (2005). Nasal mucoadhesive drug delivery: Background, applications, trends and future perspectives. *Advanced Drug Delivery Reviews, 57*(11), 1640–1665.
U.S. Food and Drug Administration. Nasonex Product Information. http://www.accessdata.fda.gov/drugsatfda_docs/label/2002/20762s11lbl.pdf.
Zhang, Z., Kim, C. S., & Kleinstreuer, C. (2006). Water vapor transport and its effects on the deposition of hygroscopic droplets in a human upper airway model. *Aerosol Science and Technology, 40*(1), 1–16.